LA-UR-99-5889
Approved for public release; distribution is unlimited.

Title: **Modeling Stress-Induced Damage from Impact Recovery Experiments**

Author(s): Robert P. Swift, Carl R. Hagelberg, Ted C. Carney, Doren Greening and Michael Hiltl

Submitted to:

http://lib-www.lanl.gov/la-pubs/00796582.pdf

Proceedings of the ETCE/OMAE 2000 Joint Conference:
Energy for the New Millennium
February 14-17, 2000, New Orleans, LA

PR - 040

MODELING STRESS-INDUCED DAMAGE FROM IMPACT RECOVERY EXPERIMENTS

Robert P. Swift, Carl R. Hagelberg, Ted C. Carney, and Doren Greening
Los Alamos National Laboratory, EES Division, Los Alamos, NM 87545

Michael Hiltl
Lawrence Livermore National Laboratory, Physics Directorate, Livermore, CA 94550

ABSTRACT

We present results from mesoscale modeling of impact recovery experiments on Berea sandstone using a hybrid Smooth Particle Hydrodynamic (SPH) and Discrete Element Method (DEM) approach. Each grain is represented with clusters of particles providing explicit representation of the grain/pore structure obtained from scanning electron microscope (SEM) and synthetic images. The modeling accounts for the influence of pore fluid and illustrates how grain/pore heterogeneity under dry and saturated states affects the evolution of grain damage behavior. The results show characteristics of the phenomena that are observed in impact recovery experiments. An increase in grain damage is associated with an increase in stress level and pulse duration. The grains in dry samples are extremely and irregularly fragmented and show extensively reduced porosity. Less grain damage and higher porosity are observed in saturated samples. The influence of pore fluid mitigates the interaction between grains, thus reducing fragmentation damage. This modeling approach in concert with experiments offers a unique way to understand dynamic compaction of brittle porous materials.

INTRODUCTION

Formation damage caused by perforating with shaped charges has long been recognized as major cause of inefficiency for well productivity (Klotz et al, 1974, Behrmann et al, 1991, Hsia et al, 1991, and Blok et al, 1996). This damage and its effects are manifested in several ways: 1) The breakdown of inter-grain cementation in consolidated rock creates particulates and generates paths for their transport. 2) Grain fragmentation caused by grain-grain interaction result in extremely small sized particulates known as fines. 3) The mobilization and intrusion of these fines into pore throats cause localized suppression of flow. These damage effects modify the local stress field and mechanical properties of the rock, often hinder hydrocarbon production and or fluid injection, cause uncertainty in fracture breakdown conditions, and impair gravel packing and frac-packing treatments. Several experimental investigations have tried to define and correlate the major cause of the damage, which is purported to be grain fragmentation caused by the intense stress delivered by the penetrating jet to induce violent grain-grain interactions. Perforation experiments by (Saucier and Lands, 1978) found fines very profusely near the tunnel walls, while experiments by (Pucknell and Behrmann, 1991) showed significant grain fragmentation existed beyond the tunnel walls. (Snider et al, 1997) measured particle size distribution in material recovered from perforated loose sand samples and related the revised size distribution to shaped-charge designs.

One aspect of these experiments is the difficulty to relate the degree of damage created in the rock fabric to a cause i.e., the stress and load duration imparted by the shaped-charge jet. The present paper attempts to address this shortcoming by modeling the grain damage observed from definitive experiments where the stress loading is fairly well known, such as that of gas-gun impact recovery experiments. (Hiltl et al, 1999a,b and Hagelberg et al, 1999) discuss these experiments and analyses of the damage observed from SEM images performed on samples of Berea sandstone. Here, we discuss numerical simulations using a hybrid technique that combines the SPH and DEM techniques to explicitly model, on a grain-pore scale, the dynamic interactions of grains undergoing fracture and fragmentation resulting from impact loading. The SPH method employs collocated particles to define a Lagrangian continuum and was originally formulated for the treatment of astrophysical problems (Gingold and Monaghan, 1977). It has been used over the past decade to model solid mechanics problems such as bomb-case fragmentation (Randles et al, 1995), impact events (Stellingwerf and Wingate, 1992), and brittle fracture (Mandell and Wingate, 1995 and Hiermaier and Riedel, 1997). The DEM approach originated as a technique for describing behavior of granular assemblies, in which an element is treated as a rigid object having Hertzian contact interactions with other elements (Cundall and Strack, 1979). It has been applied to a wide range of applications (Williams and Mustoe, 1993). Recently, simulations of dynamic brittle materials (Potapov and Campbell,

1997 and Bolander and Saito, 1998) have been conducted, in which the element interactions approximate a more flexible Hookian elastic-continuum behavior that provides explicit tensile failure (i.e., debonding) to occur between adjacent elements.

We have implemented into the SPHINX code (Crotzer et al, 1995) a hybrid SPH/DEM approach to model the dynamic behavior of heterogeneous grain-pore structures. Clusters of DEM bonded triangular elements that have elastic-equivalent interactions and a brittle fracture feature represent the grains. SPH particles portray the continuum pore-fill material, the impactor, and the recovery capsule. Our calculations are for two-dimensional representations of the grain-pore structure and illustrate realistic character associated with heterogeneous material behavior. Work to obtain three-dimensional reconstruction of the grain-pore structure from X-ray Computed Micro Tomography (XCMT) (Cole et al, 1996) and SEM images combined with synthetic representations is ongoing. The simulation results capture the complex phenomenology associated with impact loading and portray the character of the damage similar to that observed in SEM images of samples recovered from impact experiments. An increase in grain damage is associated with an increase in stress level and pulse duration. The grains in dry samples are extremely and irregularly fragmented and show extensively reduced porosity. Less grain damage and higher porosity are observed in saturated samples, due to the influence of pore fluid mitigating the interaction between grains.

Earlier simulations (Swift et al, 1998) using SPH particles for both the grains and pore-fill material did not exhibit fragmentation as clearly as the present hybrid approach does. The combining of SPH particles with DEM elements provides a way to take advantage of the strengths of each. This approach, in concert with definitive experiments, offers a unique way to examine shock-induced grain damage, correlate brittle damage modeling with known stress levels and pulse duration, better understand compaction of porous materials, and to provide an avenue for scaling constitutive behavior at the meso-scale to the macro-scale. Application to simulate perforation should enhance understanding of formation damage resulting from perforation completion treatments and possibly lead to ways to alleviate such damage according to site specific properties.

RECOVERY EXPERIMENTS AND ANALYSIS

A diagram showing the experimental setup for the impact recovery system is shown in Figure 1. Briefly, a single-stage light-gas gun with a bore diameter of 35 mm loads samples of Berea sandstone. These samples (properties given in Table 1, Zhang et al, 1990) have a diameter of 22.4 mm and a thickness of 15 mm. Impact stress for both dry and water-saturated conditions ranged from 1.3 GPa to 9.8 GPa. Pulse duration was either 1 μs or 2 μs. Finite-element macro design calculations performed for the dry case showed that the normal stress experienced at the front of the rock sample was approximately 38% lower than at the impact face. Stress attenuation through the sample was sufficient to indicate possible damage degradation from the front to the back of the sample. No finite-element calculations for the saturated case were performed, but impedance considerations at the capsule-sample interface indicated that reduction in stress from the impact face to the front of the sample would be about 29 percent. Recovered samples were cut in two halves. Particle size distribution was obtained on one half using a Microtrac-X100 laser particle size analyzer. A Noran Instruments Automated Digital Electron Microscope to produce digital SEM images was performed on the other half. XCMT images were obtained on the undamaged material and on some of dry shocked samples at the National Synchrotron Light Source at Brookhaven National Laboratory. More details of the gas-gun impact recovery experiments and on some of the analyses procedures are given by (Hiltl et al, 1999a,b)

Porosity:	21.92%
Bulk density:	2.077 g/cm^3
Grain density:	2.631g/cm^3
Average grain size:	0.14 mm
Modal analysis [Ref 22]:	75% quartz, 10% clay, 10% feldspar,5% calcite

Table 1: Properties of Berea sandstone.

Particle size distributions were obtained at several depths of recovered samples using the Microtrac-X100 angular light scattering technique. Material at each depth was measured three times and the results were used to calculate an average grain size. The measurements showed a clear grain size reduction in all impact loaded samples when compared to the undamaged material. Figure 2 compares the grain size distribution of undamaged material with that of dry and wet samples impacted at a stress level of 6.1 GPa in the regions near the front and rear of the samples. The peak sizes are 148 μm for the undamaged sample, 65 μm and 88 μm for the front and rear regions of the damaged dry sample, and a 105 μm for both front and rear regions of the damaged wet sample. For all the dry samples analyzed, a smaller grain size is noted in the impact region of the sample than in the rear region, consistent with the SEM observations below. We speculate this to be caused by stress attenuation through the sample leading to a less violent interaction of grains torward the rear of the sample. However, the wet samples show a reduced size relative to the undamaged size, but with little variation noted from front to back.

The SEM imaging of the recovered samples provides a database for assessing visual and statistical differences between areas of a given sample, and between samples subjected to different load amplitudes and pulse duration. The visual data provides a good qualitative way to correlate with mesoscale modeling, while the statistical data will provide a more quantitative comparison. Figure 3 shows five back scattered SEM images of Berea sandstone for undamaged and for dry-damaged and saturated-damaged near the front and rear of the sample. Both the dry and saturated samples were impacted with a 2μs, 6.1 GPa pulses at the capsule face. In the undamaged sandstone (Fig 3a), the shape of the grains and pores are irregular. The majority of the pores are interconnected. In some grains, pre-existing cracks can also be observed. For the dry sample near the impact surface (Fig 3b), most all the grains are extremely fragmented and irregular and the pores in this region are closed. This is caused by the stress wave driving grains into each other as it propagates through the sample. Similarly to the particle size data above, porosity is more evident near the rear of the sample and the grains are less fragmented (Fig 3c), again indicative of the stress wave being attenuated. Compared to the dry sample, the grain damage in the water-saturated sample (Fig 3d and 3e) is far lower and the reduction of the porosity significantly less. This is a result of the pore fluid cushioning the interactions between grains. Also, the difference in the grain damage between the front and rear of the wet sample is not as great as observed in the dry sample, indicative of less attenuation for saturated samples. These comparative results for dry and wet conditions are also typical for other stress levels. The statistical analyses of these and other images are more thoroughly discussed by (Hagelberg et al, 1999).

HYBRID SPH-DEM APPROACH

SPH is a Lagrangian, mesh-free method in which material elements are represented by mass points, known as particles, and are governed by the continuum equations of motion and constitutive models. Each particle functions with an interpolation function, W, which has a domain of interaction, 2h, with neighboring particles **(**Figure 4**)**, where h is the smoothing length. SPH is a collocated method i.e., values of velocity, density,

deformation rate, acceleration and energy that are obtained through interpolation with neighbor particles, along with stresses obtained from specific constitutive representations, are particle centered. The SPH approach combines the features of precise material tracking traditionally obtained only with Lagrangian methods, and that of the freedom of flow, traditionally obtained only with Eulerian methods. Thus, advection problems inherent to Eulerian formulations do not occur and mesh tangling problems typical of Lagrangian formulations are alleviated. SPH particles exist only where actual material exists, precluding the need to zone up volumes of empty space that mesh-based methods usually require. Thus, the particulate nature of SPH easily accounts for large deformation and accommodates the mixing of multi-materials in a more natural way. Excellent overviews of the approach (Swegle et al, 1995 and Randles and Libersky, 1996) discuss some of SPH strengths and limitations.

DEM is a method that has been applied to granular flow processes and brittle fracture applications where large motions occur or where heterogeneous surface interactions are dominant. An element is treated as a rigid body volume with translation and rotation degrees of freedom and interacts with other elements via, Hertzian or spring force-displacement laws to maintain a balance of momentum. Objects may be represented either as single elements or cluster of elements that are bonded and interact with other element clusters through surface contact forces. Recently, the method has been advanced to approximate dynamic fracture where element interactions behave equivalently to that of an elastic continuum with tensile debonding of elements providing explicit fracture (Potapov and Campbell, 1997).

For the modeling grain-grain interactions of brittle behavior in sandstone, we combine the DEM and SPH approaches in the SPHINX code (Crotzer et al, 1995). Each grain consists of a cluster of triangular elastic-continuum equivalent elements, (Figure 5a), that are angular and/or oval shaped, while the pore-fill material, impactor and recovery capsule are represented by continuum SPH particles. DEM elements experience normal and shear translation forces along their interfaces in terms of pair-wise relative displacement and experience moments in terms of the evolving vector offset of the translation forces between element centroids, (Figure 5b). These forces are determined from stresses and strains at element interfaces that obey Hooke's isotropic law of elasticity. The process is to estimate the strain tensor at the elemental interface, which permit stresses to be evaluated, and then estimate forces by assuming they act over the area of the triangular interface. Surface interactions between DEM elements or between a DEM element and a SPH particle are treated by a penalty method.

Fracture modeling considers the normal stress at the interface between elements. If the normal force F_n value exceeds a threshold value, σ_{th}, a crack is assumed to grow at a fixed rate. Formally, if

$$F_n > A_{eff}\,\sigma_{th} \quad ,$$

then

$$A_{eff} = A - \gamma \Delta t \quad ,$$

where **A** denotes the initial interfacial tension area and γ is a specified rate parameter for fracture area reduction. The triangle elements are tessellated giving varying element interface area, and hence, a somewhat random tensile force threshold. As the effective area decreases the tensile force is reduced until complete fracture occurs. This reduction in area has the effect of softening the elastic model. When the normal strain is compressive the original area is used, but the effective tension area is always used in calculation of the shear force. This DEM method yields explicit brittle fracture and the coupling with SPH provides a way to take advantage of the strengths of each approach. More complete details of this DEM approach and fracture modeling are given by (Greening, 1999).

IMPACT SIMULATIONS

Representations of heterogeneous grain-pore structures for impact loading simulations are created to be similar in character to that of reservoir rock obtained from SEM and XCMT images. Figure 6a shows reconstituted and synthetic grain-pore structures that are used for SPH/DEM plate impact simulations. The synthetic structure is an adaptation of the method given by (Tacher et al, 1997) that allows the grain size distribution and regularity of the boundaries to be varied. The reconstituted structure directly imitates a SEM image of undamaged Berea sandstone in Figure 6b. The porosity of this structure is about 20 percent and the pores (black regions) can be dry, fluid-filled, or filled with any other material. At present, the reconstitution procedure is manual and while it provides good 2-D representations it is somewhat tedious, and extending it to a 3-D grain-pore representation is very tedious. We are currently pursuing ways to automate reconstruction of real grain-pore structures in 3-D.

For the following simulations, we employ the synthetic grain structure having an area occupied by the grains of 4 sq-mm and a porosity of about 23 percent. The impactor and capsule are modeled as elastic-plastic with 6061-T6 aluminum properties with density = 2.7 g/cc, Poisson's ratio = 0.35, bulk modulus = 78 GPa and plastic yield of 0.3 GPa.. The grains are modeled as pure sandstone quartz with elastic properties with density = 2.65 gm/cc, Poisson's ratio = 0.32, and bulk modulus = 54 GPa. The fracture parameters for the quartz brittle failure model are σ_{th} = 0.3 GPa and γ = 1e4 sq-cm/s. Fluid-filled pores are modeled with a water tabular EOS (Crotzer et al, 1995) with an initial density = 1.0 gm/cc. The total number of particles for the dry and saturated cases is 24,800 and 35,300, respectively. There are 160 grains with a total of 14,400 DEM elements. The top and bottom surfaces of the capsule are treated as roller boundaries that allow motion along but not across them. The rear boundaries of the capsule and impactor plate are free surfaces.

Illustrations for the evolution of simulated grain fragmentation for an impact velocity of 0.88 km/s are shown in Figures 7 and 8 for dry and wet cases, respectively. The dotted line represents the position of the stress wavefront at the times indicated. The irregularity the front for the dry case shows the influence of the heterogeneous grain-pore structure on stress wave propagation. An even front with no spatial variation would occur for a uniform media. Quite noticeable for the dry case is the compaction of the pore space occurring behind the wavefront. As the fragments form they are rearranged in a manner that removes the pore space, forming regions of approximate grain density quartz. This is indicative of the character of grain damage observed on recovered samples of dry sandstone as shown in Figure 3. In contrast, irregularity of the wavefront for the saturated grain-pore structure, Figure 8, is still quite evident but much less than for the dry case. It advances faster into the structure because the pore fluid provides propagation between grains. The degree of grain fragmentation is significantly reduced, again in accord with observations of recovered wet samples in Figure 3. Also, what was compaction for the dry case is in turn manifested as expansion for the saturated case. The reduction in fragmentation is attributed to the cushioning influence that the pore fluid provides between grain-grain interactions. For the dry case this cushioning does not exist and more severe grain-grain interactions occur. The expansion observed in the saturated structure is caused by stress-wave induced buildup of pore pressure and the more rapid unloading of the stiffer grains relative to the less-stiff pore fluid. This eventually leads to the grains being pushed apart and causes the capsule to expand. This was observed in the wet recovery experiments, and in some of these tests, the aluminum recovery capsule failed from the inside out. Also, of interest to note, is the

increased fracturing observed late for the wet case, Figure 8c, resulting from the reflected wave off the capsule rear free-surface. The reality of this influence on damage in the recovery experiments is at present unproven.

Figure 9 illustrates simulated grain damage for dry and wet conditions for impact velocities of 0.4 km/s and 0.88 km/s, respectively. Noticeably more damage and compaction is obtained for the higher impact velocity in the dry case. Slightly more damage and expansion is obtained for the higher impact velocity in the wet case. Also noticeable is the extreme angularity of the fragments for the dry cases relative to those for the wet cases. All of these simulated results are consistent in a qualitative sense with observations obtained from data analyses of the impact recovery experiments (Hagelberg et al, 1999).

To obtain a quantitative measure of the simulated damage in Figure 9, we first colored all the grains and grain fragments a medium gray, the grain and fragment boundaries black, and the pore space white. We processed these images with *NIH Image* to obtain the area of each DEM fragment created in the simulations. The log-normal distributions of this data in terms of fragment size (i.e., taken as the square root of the area distribution) are shown in Figure 10. The distribution curves are represented as follows: small dashed curve for the initial grain-pore structure (Figure 8a), large dashed curve for the dry, V = 0.4 km/s case (Figure 8b), solid curve for the dry, V = 0.88 km/s case (Figure 8c), medium dashed curve for the wet, V = 0.4 km/s case (Figure 8d), and dash-dot curve for the wet, V = 0.88 km/s case (Figure 8e). The peak value for the initial distribution is 161 μm with a range between 50 μm and 210 μm. The peak size values are shifted to smaller size values and the distributions show more abundance toward smaller sizes as the impact velocity is increased and for dry pores relative to wet pores. The peak size values are 19 μm for the hi-V-dry, 21 μm for the low-V-dry, 30 μm for hi-V-wet, and 165 μm for the low-V-wet cases, respectively. It is observed that smaller grains tend to fragment more for the low-V-wet case and that bimodal distributions for both the hi-V-wet and low-V-wet cases occur. These features are in accord with observations from impact recovery experiments, where bimodal distributions were obtained for the wet and dry tests, being much more evident for the wet case (see Figure 2).

CONCLUSIONS

We have demonstrated the use of a hybrid numerical approach combining Smooth Particle Hydrodynamics with the Discrete Element Method as a way to model, on a grain-pore scale, the dynamic interactions of quartz grains resulting in grain fragmentation from stress wave loading. Mesoscale simulations of plate impact recovery experiments on Berea sandstone show the influence of explicit heterogeneity of void-dry pore space and water-filled wet pores on the stress wave propagation and on the fragmentation damage induced into the grain-pore structure. Several features captured by the grain fragmentation simulations are similar to that observed from SEM images and particle size analyses of recovered impact samples. For example, significant increase in fragmentation damage is obtained for higher impact velocities and for dry relative to wet cases (i.e., the 0.88 km/s impact loading relative to 0.4 km/s loading shown). This leads to simulated particle size distribution in qualitative accord with measured data from recovered samples. The correlation between the SPH/DEM simulations and the recovery experiments is presently qualitative. Questions on the adequacy of the size of the simulations (i.e., currently 4 sq-mm), of the fracture model, using actual grain-pore, etc., all need to be addressed.

The explicitness and the fidelity that the hybrid SPH/DEM simulations portray of the fracturing process appear very realistic and provide motivation to pursue further development. Although the grain-pore scale simulations are two-dimensional, they capture the essence of how damage to the rock fabric may occur from perforation-type stress wave loading They illustrate the complexity of how heterogeneity affects stress wave behavior which in turns affects damage evolution. These results along with perforation experiments suggest that a number of aspects such as grain size, porosity, grain angularity, smoothness, cementation, clay content, fluid content, unconsolidation, etc., may all play a role in perforation-induced damage. We believe that authentic representations of three-dimensional grain-pore structures are needed to properly evaluate these effects. Exercising grain-pore scale simulations over a wide range of geophysical parameters will help calibrate and provide more reliable macro-continuum damage descriptions. These employed in concert with perforation phenomenology experiments will hopefully lead to improvement of perforation treatment designs.

REFERENCES

Behrmann, L.A., Pucknell, J.K., Bishop, S.R. and Hsia, T.Y., 1991, "Measurement of Additional Skin resulting From Perforation Damage," SPE Paper 22809.

Blok, R.H.J., Welling, R.W.F, Behrmann, L.A. and Venkitaraman, A., 1996, "Experimental Investigation of the Influence of Perforating on Gravel Pack Impairment," SPE Paper 36481.

Bolander, J.E. and Saito, S., 1998, "Fracture analyses using sping networks with random geometery," *Eng. Fracture Mech.* ***61****, 569-591*.

Coles, M.E., Hazlett, R.D. Spanne, P., Muegge, E.L. and Fur, M.J., 1996, "Characterization of Reservoir Core Using Computed Microtomography," *SPE Journal* ***1, 3,*** *295-302*.

Crotzer, L.A., Dilts, G.A., Knapp, C.E., Swift, R.P., and Wingate, C.A., 1995, "SPHINX Manual," Version 11.0, Los Alamos National Laboratory Document LA-13436-M.

Cundall, P. A. and Strack, O. D. L., 1979, "A discrete numerical model for granular assemblies," *Geotechnique, **29**, 47-65*.

Gingold, R. A., and Monaghan, J. J., 1977, "Smoothed Particle Hydrodynamics: Theory and Application to Non-spherical Stars," *Mon. Not. Roy. Astr. Soc.* ***181****, 373-389.*

Greening, D., "The Basis of Discrete element Modeling of Brittle elastic Material," (in preparation), (1999).

Hagelberg, C. R, Hiltl , M., Swift, R. P., and Nellis, W. J., 1999, "Analysis of Shock Damage to Sandstone Using SEM Images of Samples from Impact Recovery Experiments," *Proceedings of the ETCE/OMAE 2000 Joint Conference: Energy for the New Millennium*, this issue.

Hiermaier, S. and Riedel, W., 1997, "Numerical Simulation of Failure in Brittle Materials using Smooth Particle Hydrodynamics," *International Workshop on New Models and Numerical Codes for Shock Wave Processes in Condensed Media*, presented at St. Catherine's College, Oxford, UK.

Hiltl, M., Swift, R.P., Hagelberg, C.R., Carney, T. C., and Nellis, W.J., 1999a, "Shock-Recovery Experiments of Sandstone Under Dry and Water-Saturated Conditions," *Shock Compression in Condensed Matter* edited by M. D. Furnish, APS Conference Proceedings.

Hiltl, M., Hagelberg, C. R., Swift, R. P., Carney, T. C., and Nellis, W. J., 1999b, " Dynamic Response of Berea Sandstone Shock-loaded Under Dry, Wet and Water-Pressurized Conditions," *AIRAPT-17 International Conference on High Pressure Science and Technology*, AIRAPT Conference Proceedings.

Hsia, T-Y. and Behrmann, L.A., 1991, "Perforating skin as a Function of Rock Permeability and Underbalance," SPE Paper 22810.

Klotz, J.A., Kruger, R.F. and Pye, D.S., 1974, "Effect of Perforation Damage on Well Productivity," *J. Pet. Tech* and SPE Paper 4792.

Mandell, D. A., Wingate, C. A., 1995, "Numerical Simulations of Glass Impacts Using Smooth Particle Hydrodynamics," *APS Topical Conference on Shock Compression in Condensed Matter*.

Pucknell, J.K. and Behrmann, L.A.: 1991, "An Investigation of the Damaged Zone Created by Perforating," SPE Paper 22811.

Potapov, A.V. and Campbell, C.S., 1997, "The Two Mechanisms of Particle Impact Breakage and the Velocity Effect," *Powder Technology, 93, 13-21*.

Randles, P. W., Carney, T. C., and Libersky, L. D., 1995, "Continuum Dynamical Simulations of Bomb Fragmentation," *Pro. 15th Int. Symp. Ballistics*, Jersualem, Israel.

Randles P.W. and Libersky, L.D., 1996, "Smoothed Particle Hydrodynamics: Some Recent Improvements and Applications," *Comp.Meth.Appl.Mech.Eng.* ***139****, 375-408.*

Saucier, R.J., and Lands, J.F., 1978, "A Laboratory Study of Perforations in Stressed Formation Rocks," *J. Pet. Tech., 1347*.

Snider, P.M., Benzel, W.M., Barker, J.M., and Leidel, D.J., 1997, "Perforation Damage Studies in Unconsolidated Sands: Changes in Formation Particle Sizes and the Distribution as a Function of Shaped Charge Design," SPE Paper 38635.

Stellingwerf, R. F. and Wingate, C. A., 1992, "Impact Modeling with Smooth Particle Hydrodynamics," *Los Alamos National Laboratory Report LA-UR-92-1981*.

Swegle, J.W., Hicks, D.L., and Attaway, S.W, 1995, "Smoothed Particles Hydrodynamics Stability Analysis," *J. Comp. Phys.* ***116****, 123-134*.

Swift, R.P., Behrmann, L.A., Halleck, P.M., and Krogh, K.E., 1998, "Micro-Mechanical Modeling of Perforating Shock Damage," SPE Paper 39458, *Proc of Int. Sym. on Formation Damage Control*.

Tacher, L., Perrochet, P., and Parriaux, A., 1997, "Generation of Granular Media," *Transport in Porous Media, 26, 99-107*.

Williams, J. R., Mustoe, G. G.W., 1993, editors. *Proceedings of the 2nd International Conference on Discrete Element Methods (DEM).* IESL Publications, Dept. of Civil and Environmental Engineering, Massachusetts Institute of Technology.

Zhang, J., Wong, T.F., Yanagidani, T., Davis, D. M., 1990, *Mechanics of Materials,* ***9****, 1-15*.

This work was supported by U. S. Department of Energy under Contract No W-7405-ENG-36

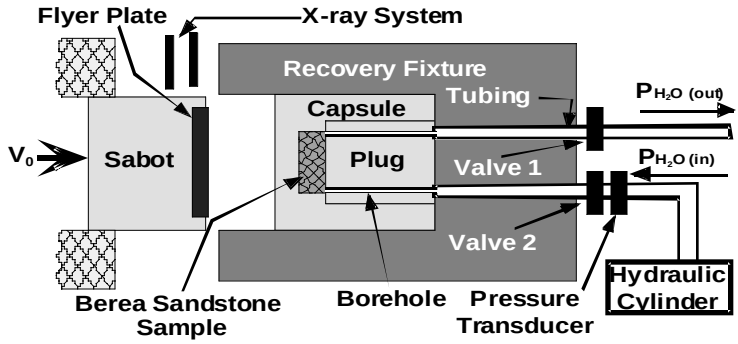

Figure 1. Experimental configuration for gas-gun recovery tests.

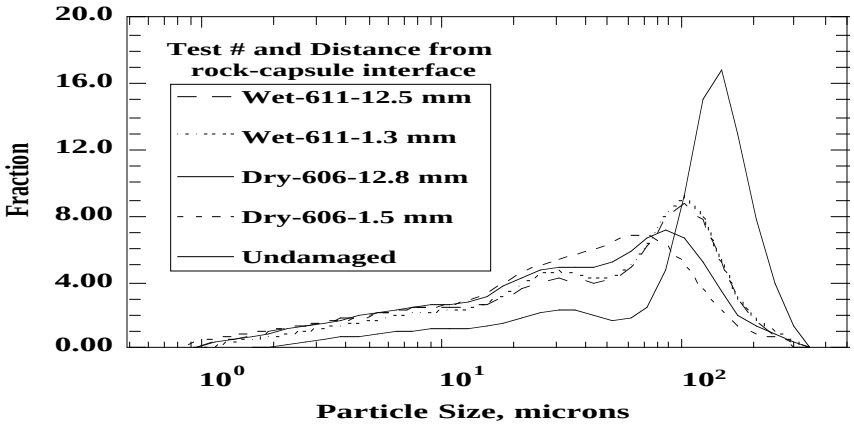

Figure 2. Laser particle analysis for dry and wet samples shocked at 6.1 GPa.

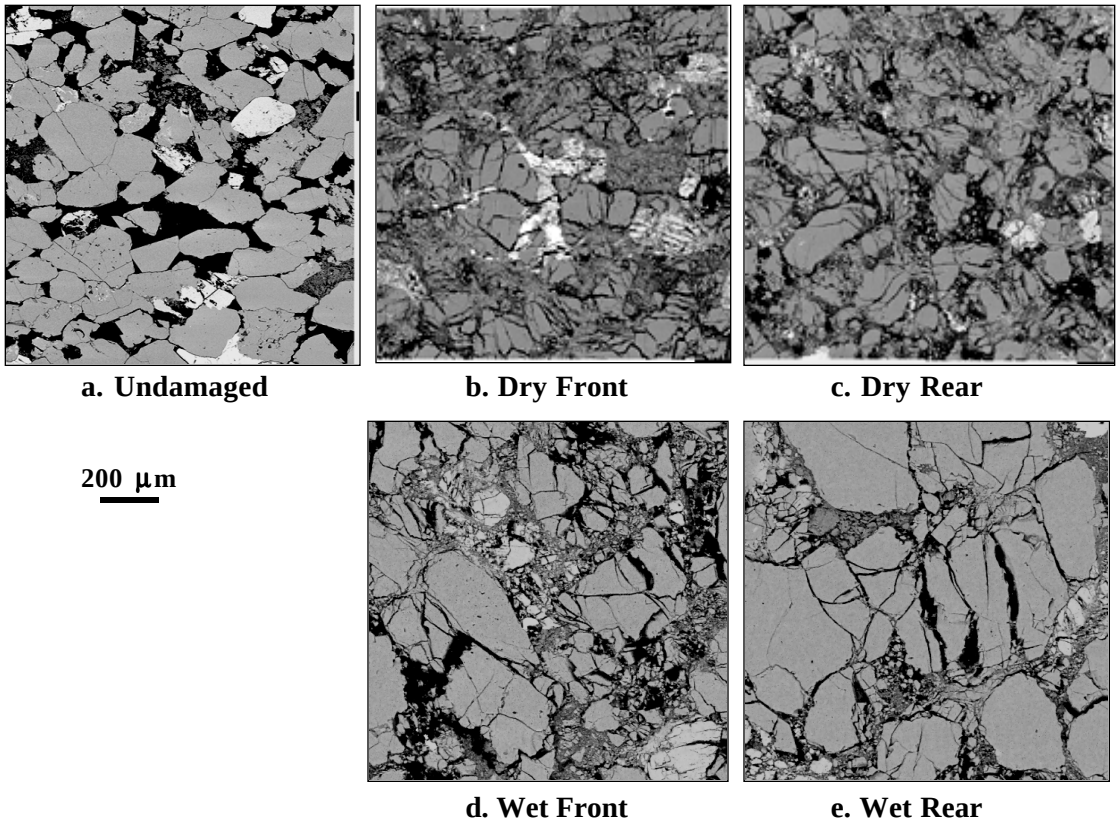

Figure 3. SEM images of (a) undamaged and impact surface load of 6.1 GPa, (b) dry near front of sample, (c) dry near rear of sample, (d) wet near front of sample, and (e) wet near rear of sample.

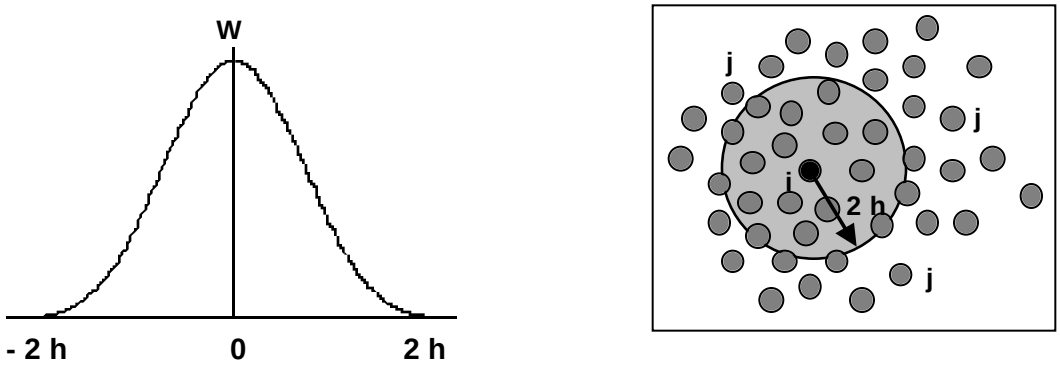

Figure 4. Cubic B-Spline Kernel approximation and domain of interpolation dependence, 2h, for SPH particle i on particles j.

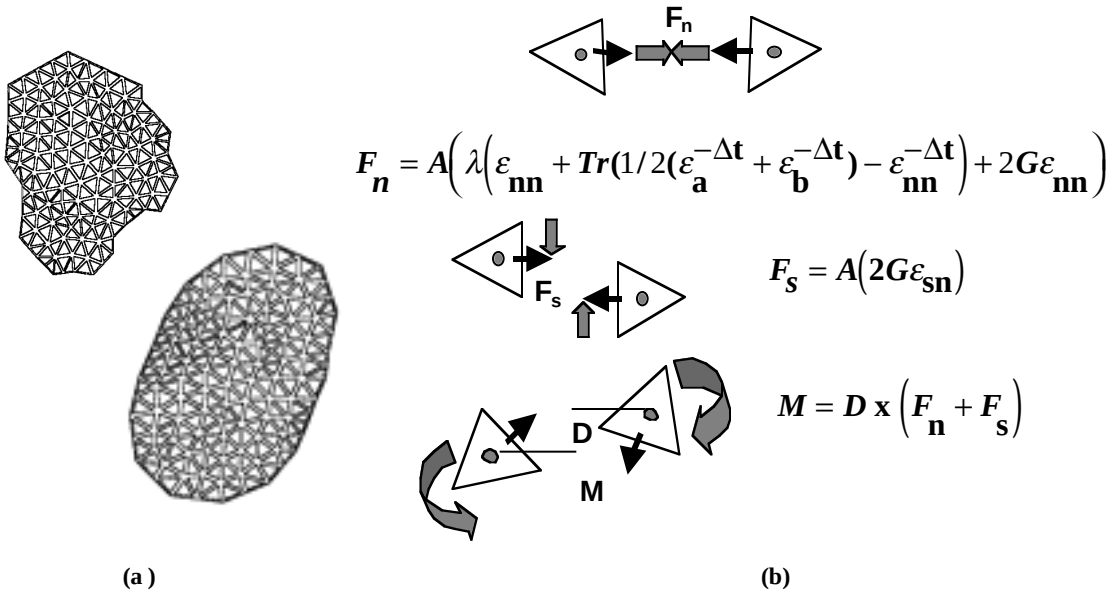

$$F_n = A\left(\lambda\left(\varepsilon_{nn} + Tr(1/2(\varepsilon_a^{-\Delta t} + \varepsilon_b^{-\Delta t}) - \varepsilon_{nn}^{-\Delta t}\right) + 2G\varepsilon_{nn}\right)$$

$$F_S = A\left(2G\varepsilon_{sn}\right)$$

$$M = D \times \left(F_n + F_s\right)$$

Figure 5. (a) Angular and oval grains consisting of triangular DEM elments. (b) Force interactions for DEM elements, where F_N, F_S, and M are the normal force, shear force, and moment acting on element pair with interface area A. The Lame constants are λ and G, with ε_{nn}, ε_{sn}, ε_a, and ε_b as the normal, shear strain and mean strains for elements a and b, respectively.

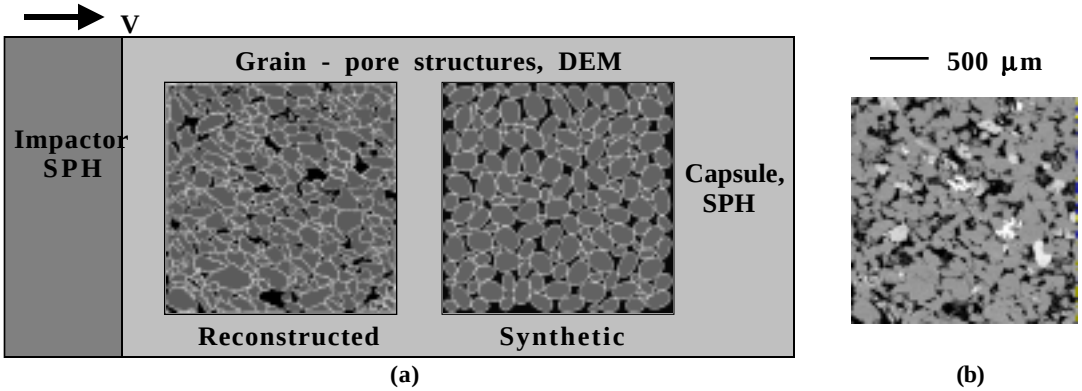

Figure 6. (a) Plate-impact configuration for SPH/DEM meso-scale damage simulations with synthetic grain-pore structure and reconstructed grain-pore structure from (b) undamaged SEM image of Berea sandstone.

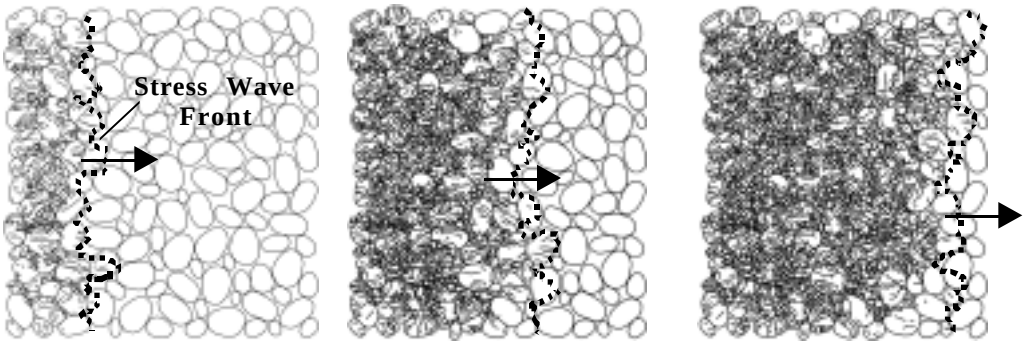

Figure 7 Evolution of grain fragmentation for meso-scale simulation of dry grains for impact velocity of 0.88 km/s. The dotted line represents the stress wave front at (a) 0.25 μs, (b) 0.50 μs, and (c) 0.75 μs after impact.

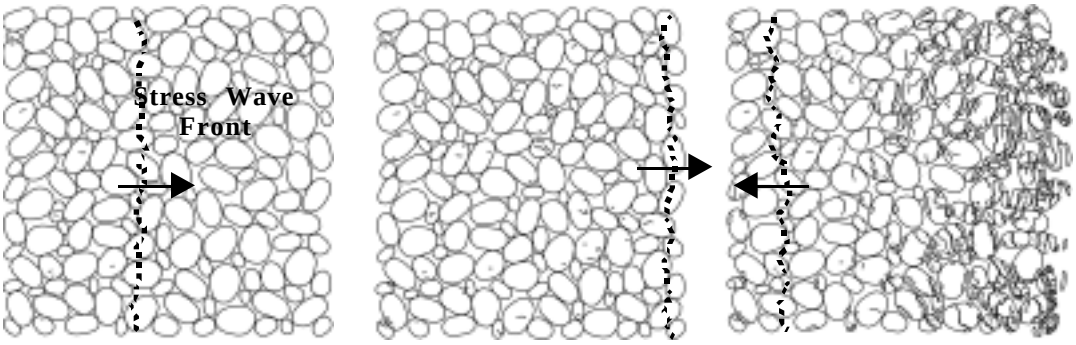

(a) 0.25 μs **(b) 0.50 μs** **(c) 1.25 μs**

Figure 8 Evolution of grain fragmentation for meso-scale simulation of dry grains for impact velocity of 0.88 km/s. The dotted line represents the stress wave front at (a) 0.25 μs, (b) 0.50 μs, and (c) 1.25 μs after impact

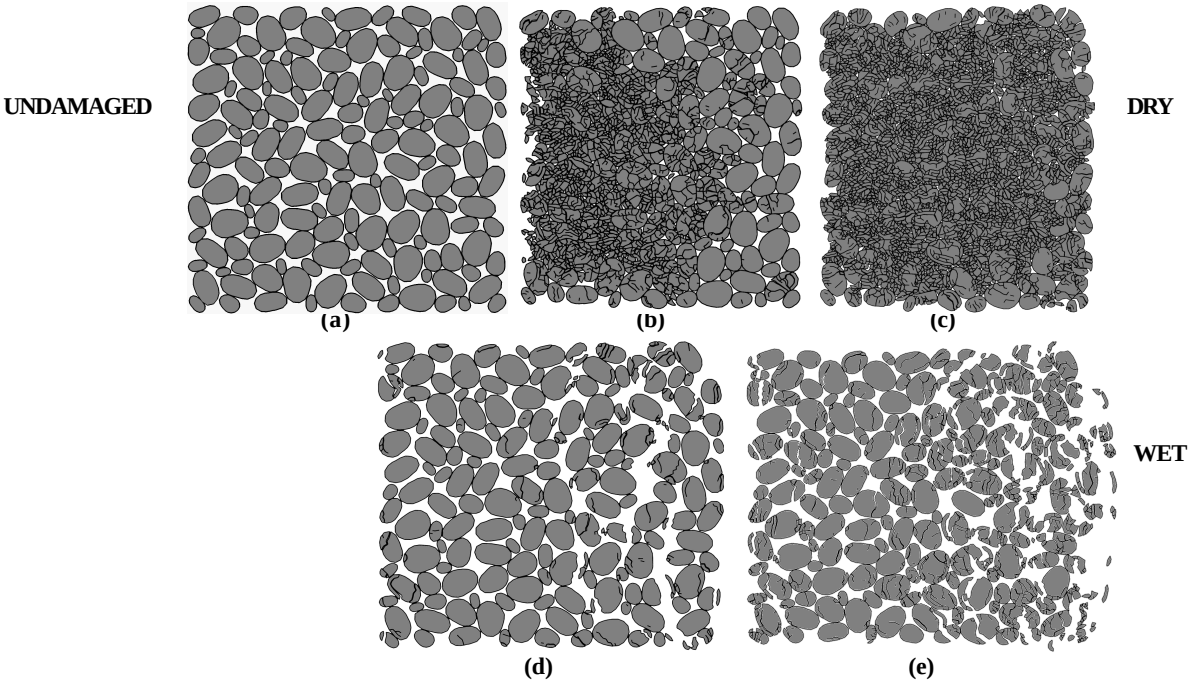

Figure 9 Comparison of grain fragmentation from meso-scale simulations. (a) Original structure, (b) Dry, V= 0.4 km/s, (c) Dry, V= 0.88 km/s, (d) Wet, V= 0.4 km/s, and (e) Wet, V= 0.88 km/s.

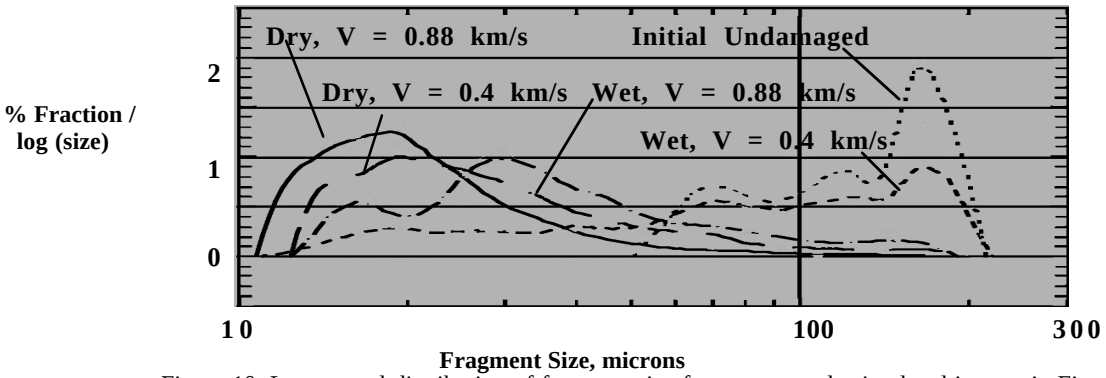

Figure 10. Log-normal distribution of fragment size from meso-scale simulated images in Figure 9